Ain Shams Engineering Journal 14 (2023) 102535

Contents lists available at ScienceDirect

Ain Shams Engineering Journal

journal homepage: www.sciencedirect.com

Numerical simulation of thermal behavior of cerebral blood vessels using computational hemodynamic method

Yutao Li [a,*], Shahab Naghdi Sedeh [b], As'ad Alizadeh [c], Maytham N. Meqdad [d], Ahmed Hussien Alawadi [e,f,g], Navid Nasajpour-Esfahani [h], Davood Toghraie [b], Maboud Hekmatifar [b]

[a] Wuhan Third Hospital, Hubei, Wuhan 430070, China
[b] Department of Mechanical Engineering, Khomeinishahr Branch, Islamic Azad University, Khomeinishahr, Iran
[c] Department of Civil Engineering, College of Engineering, Cihan University-Erbil, Erbil, Iraq
[d] Intelligent Medical Systems Department, Al-Mustaqbal University, 51001 Babil, Iraq
[e] College of Technical Engineering, The Islamic University, Najaf, Iraq
[f] College of Technical Engineering, The Islamic University of Al Diwaniyah, Iraq
[g] College of Technical Engineering, The Islamic University of Babylon, Iraq
[h] Department of Material Science and Engineering, Georgia Institute of Technology, Atlanta 30332, USA

ARTICLE INFO

Keywords:
Viscosity model
Thermal effect
Cerebral blood vessel
Non-Newtonian blood flow
Dimensionless pressure
Nusselt number

ABSTRACT

Nowadays, cardiovascular illnesses are among the leading causes of death in the world. Thus, many studies have been performed to diagnose and prevention of these diseases. Studies show that the computational hemodynamic method (CHD) is a very effective method to control and prevent the progression of this type of disease. In this computational paper, the impression of five non-Newtonian viscosity models (nNVMs) on cerebral blood vessels (CBV) is investigated by CHD. In this simulation, blood flow is supposed steady, laminar, incompressible, and non-Newtonian. The parameters of Nusselt number (Nu), dimensionless temperature (θ), pressure drop (Δp), and dimensionless average wall shear stress (DAWSS) are also investigated by considering the effects of heat generated by the body. Utilizing the FVM and SIMPLE scheme for pressure–velocity coupling is a good approach to investigating CBVs for five different viscosity models. In the results, it is shown that the θ and Δp^+ increase with increasing Reynolds number (Re) in the CBVs. By enhancing the Re from 90 to 120 in the Cross viscosity model, the Δp^+ changes about 1.391 times. The DAWSS grows by increasing the Re in all viscosity models. This increase in DAWSS leads to an increasing velocity gradient close to the cerebral vessel wall.

1. Introduction

Blood flow is made up of a combination of cells and fluid [1]. The cell part, which contains red and white blood cells and platelets, makes up 45 % of the blood volume. The fluid (plasma) part, which contains water, salts, hormones, coagulants, organic and fatty substances, proteins, and sugars, makes up 55 % of the blood volume. It is also responsible for transporting the absorbed food from the gastrointestinal tract to the tissues and body cells and the excretion of waste products to the kidneys and liver [2,3]. Cerebral blood flow provides the oxygen and nutrients needed for the brain to function properly [4]. It carries blood, oxygen, and glucose to the brain. Although the brain makes up a small portion of the total body weight, it needs a lot of energy to function. Oxygen consumption is relatively high in the brain and neurons, but their storage is very low [5]. Therefore, the amount of blood vessels and capillaries in the brain tissue is very high because it can meet the need for about 55 ml of blood per minute for every 100 g of brain tissue [6–8]. The human brain needs about 15 percent of the heart's output to get the oxygen and glucose it needs. In other words, the brain needs a lot of blood circulation to maintain its health. When this circulation is impaired, the brain may be damaged, and many complications and disabilities can occur as a result. Today, one of the most significant causes of fatality, especially in developed countries, is cardiovascular disease [9,10]. Dynamic properties of blood flow play an important role in understanding and treating many cardiovascular diseases. Therefore, it is necessary to study and analyze the characteristics of blood flow in

* Corresponding author.
E-mail addresses: Liyutao7526@126.com (Y. Li), Toghraee@iaukhsh.ac.ir (D. Toghraie).

https://doi.org/10.1016/j.asej.2023.102535
Received 25 December 2021; Received in revised form 27 June 2023; Accepted 16 October 2023
Available online 27 October 2023

Fig. 1. The Schematic of the simulated CBV.

Table 1
Thermophysical characteristics of blood and vessels [26,27].

Parameter	Blood	Vessel
Density	1060 kg.m^{-3}	1190 kg.m^{-3}
Thermal conductivity	0.556 W.m^{-1}.K^{-1}	0.235 W.m^{-1}.K^{-1}
Heat capacity	3770 J.kg^{-1}.K^{-1}	3600 J.kg^{-1}.K^{-1}

the vascular sections. In many studies on the dynamic properties of blood flow, blood flow has been considered to be a Newtonian or non-Newtonian monolayer fluid. In a numerical study, Liu et al. [11] analyzed the pulsed blood flow along a sampled vessel. In their study, blood flow was considered to be Newtonian fluid, and the given vessel was assumed to be inelastic. The Navier-Stokes equations governing blood flow are solved in their study using the finite difference method. The hypothesis that blood flow is Newtonian for flow with high shear strain is agreeable, which is true for flow along vessels with an interior diameter larger than one millimeter [12–14]. On the other hand, decreased cardiovascular function leads to impaired regulation of cerebral blood flow. Therefore many studies have been done on cardiovascular disease and cerebral blood flow. Tarumi et al. [15] investigated cardiovascular factors and clinical implications for cerebral blood flow in adults. The results show that regular aerobic exercise improves cardiovascular function and better regulation of cerebral blood flow. Therefore, it reduces the risk of dementia. Matthew et al. [16] investigated the risk of cardiovascular disease and the velocity of cerebral blood flow. The results show that cardiovascular disease has different effects on moderate blood flow velocity. Also, the study of cerebrovascular reactions and arterial stiffness can contribute to brain pathology and cognitive impairment. Jennings et al. [17] investigated cardiovascular disease using cerebral blood flow. The results show that aging and cardiovascular disease lead to decreased cerebral blood flow. Moitoi et al. [18] investigated the impression of using the magnetic drug targeting at the same time as Caputo-Fabrizio fractionalized blood flow through a permeable vessel. The results showed that enhancing Re results in lessening the tendency of the drug to trap near the tumor site, whereas the pulsatile frequency presents a conflicting phenomenon. Shaw et al. [19] investigated the permeability and stress-jump effects on magnetic drug targeting in a penetrable microvessel. The results showed that the permeability of the carrier particle increases the tendency of the carrier particles to capture close by tumor position.

Maiti et al. [20] investigated the fractional order model for the thermochemical flow of blood. The results showed that blood velocity and temperature both lessen in arising values of the fractional-order parameter as the memory effect. The penetrability of the blood flow medium withstands to drive the fluid fast. Sharma et al. [21] investigated the hemodynamical analysis of MHD two-phase blood flow. The results showed that the curvature and penetrability of the arterial wall increase the risk of atherosclerosis formation, while the implication of heat source on the blood flow lower this risk. Daset al. [22] investigated the effect of hall and ion slip currents on electromagnetic blood flow conveying hybrid nanoparticles. The results show that hybrid nanoparticle concentration has an important role in the heat-conducting nature of blood which is cardinal to life support. Prakash et al. [23] investigated the effects of stenoses on the non-Newtonian flow of blood in blood vessels. The results show that stenoses size lessens the flow rate and enhance the wall shear stress as well as resistance to flow.

In this paper, the effects of the five distinct nNVMs of cerebral blood flow on Δp, DAWSS, θ, and Nu are studied. An open-source software [24] based on MRI and DICOM is used to construct a 3D computational model of the CBVs. The blood flow is treated as a single-phase fluid. The Re ranges from 30 to 120. The vessel wall is also assumed solid.

2. Numerical methods

In this numerical analysis, the effects of five different nNVMs such as Power-law, Cross, Quemada, Carreau, and Carreau-Yasuda on the parameters of Δp^{+}, DAWSS, θ, and Nu are investigated. Several approaches have been proposed so far to create 3D biological geometries. This study employs the DICOM and MRI approaches for creating 3D geometries of blood vessels. Open-source software like SimVascular [24] is utilized to make geometry from images into a 3D CAD file. The Schematic of the simulated CBV is represented in Fig. 1. The geometry creation process is briefly expressed as follows:

- Draw a path line along the length of the vessel (using xy-plane)

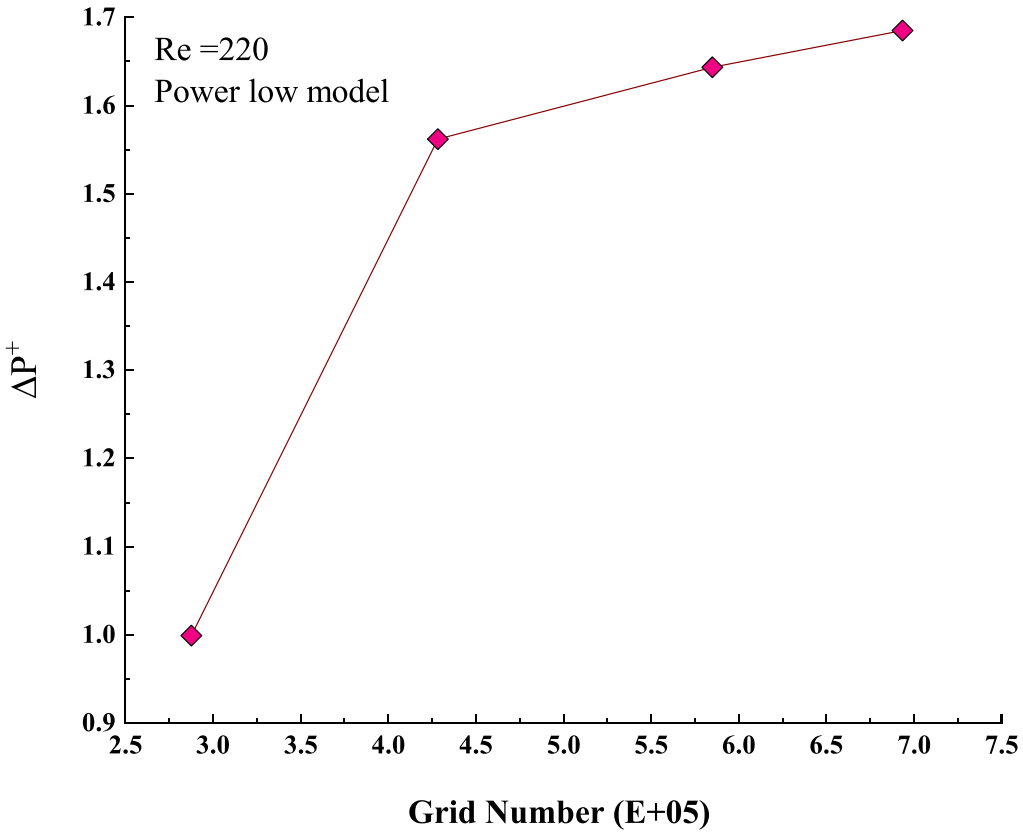

(a)

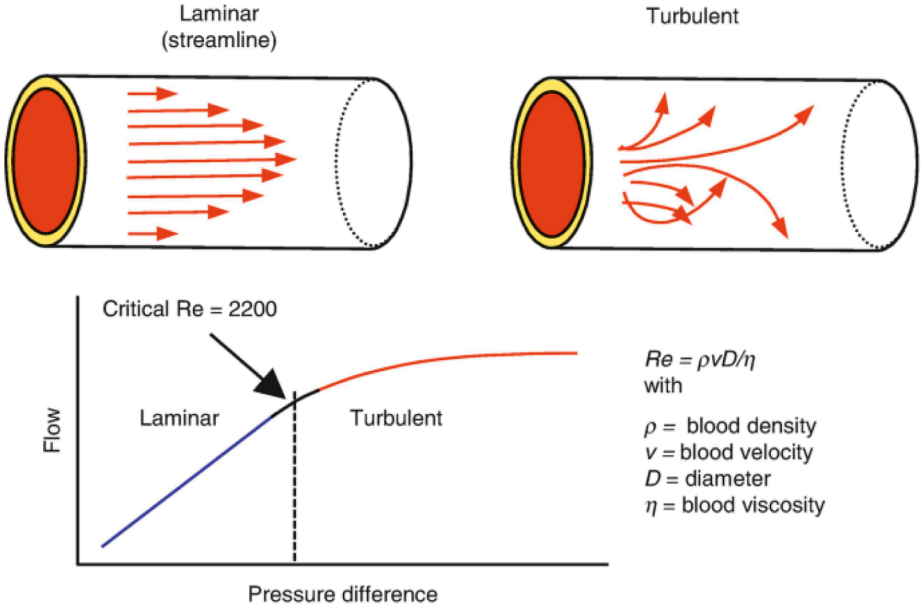

(b)

Fig. 2. A) grid independency of the 3d model of the cbvs for numerical computation, b) laminar and turbulent blood flow patterns.

- Draw a vessel wall line using images (perpendicular to xy-plane)
- Create point clouds
- Create a shell using point clouds (vessel wall)
- Create a volume of the vessel

The range of velocity for this situation of the thoracic aorta and the blood temperature is considered between 0.15 and 0.45 $m.s^{-1}$ and 309.55 K based on clinical data, respectively. The heat flux on the thoracic aorta wall is considered constant heat flux at normal daily activity. The DICOM and MRI method and SimVasular software were used

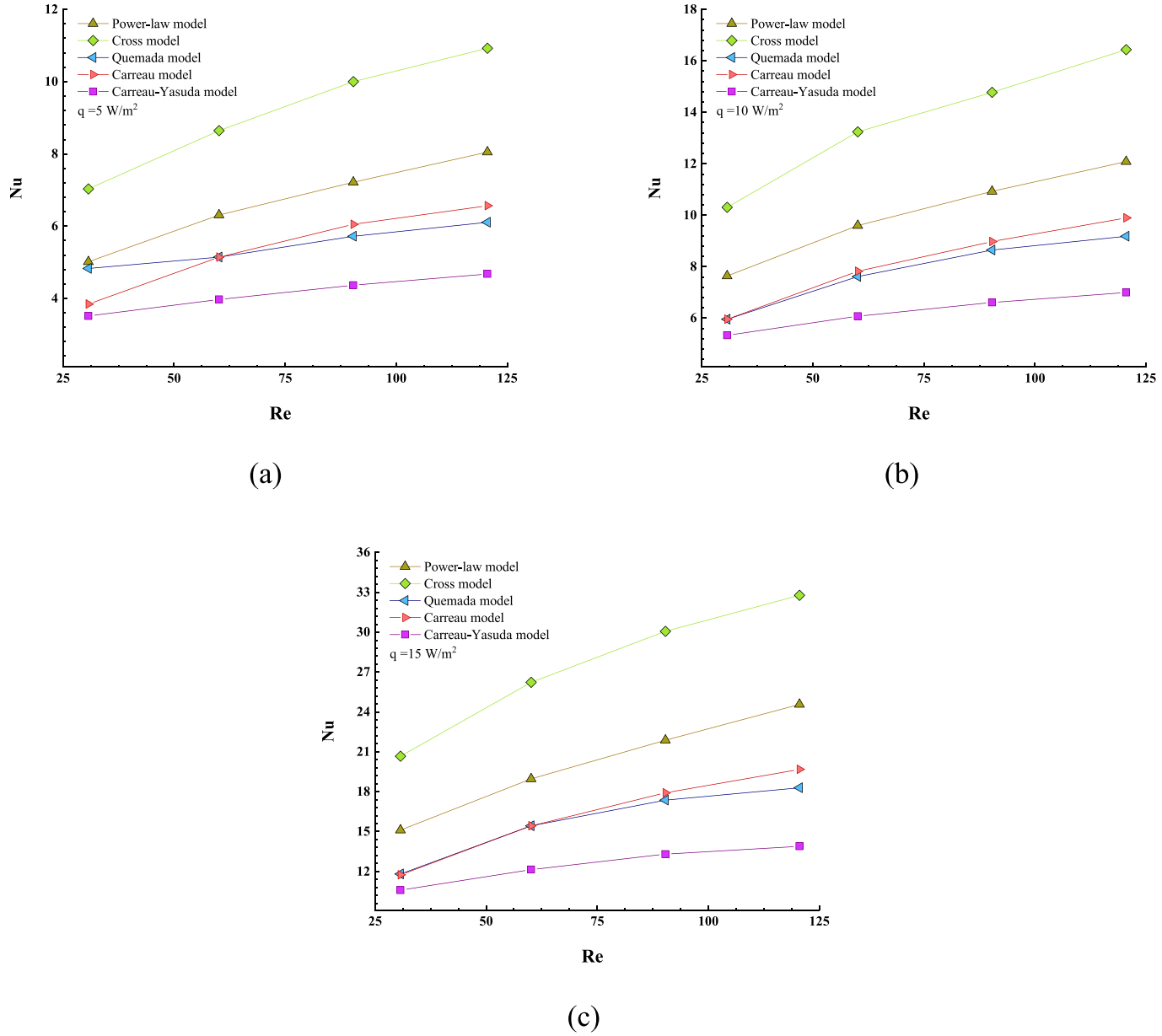

Fig. 3. Nu in terms of Re amount in the CBVs for all five viscosity.

to construct the 3D geometry of blood vessels with excellent accuracy [25]. Heat flux is also intended for three types of daily activities. The body produces this heat flux on the vessel wall. The thermophysical characteristics of blood and vessels are reported in Table 1.

In this numerical analysis of non-Newtonian blood flow for the abdominal aorta, the biological fluid is assumed a time-dependent laminar incompressible flow. The FVM and SIMPLE schemes are used to couple velocity and pressure [28]. The conversion equations, including mass, momentum, and energy equations solved by the approaches above, are represented as follows:

Continuity equation:

$$\nabla.(\rho.\vec{\mathrm{V}}) = 0 \tag{1}$$

Momentum equation:

$$\rho\left[u\frac{\partial u}{\partial x}+v\frac{\partial u}{\partial y}+w\frac{\partial u}{\partial z}\right] = -\frac{\partial p}{\partial x}+\left[\frac{\partial}{\partial x}\left(\eta\frac{\partial u}{\partial x}\right)+\frac{\partial}{\partial y}\left(\eta\frac{\partial u}{\partial y}\right)+\frac{\partial}{\partial z}\left(\eta\frac{\partial u}{\partial z}\right)\right](x-direction) \tag{2a}$$

$$\rho\left[u\frac{\partial v}{\partial x}+v\frac{\partial v}{\partial y}+w\frac{\partial v}{\partial z}\right] = -\frac{\partial p}{\partial y}+\left[\left[\frac{\partial}{\partial x}\left(\eta\frac{\partial v}{\partial x}\right)+\frac{\partial}{\partial y}\left(\eta\frac{\partial v}{\partial y}\right)+\frac{\partial}{\partial z}\left(\eta\frac{\partial v}{\partial z}\right)\right]\right](y-direction) \tag{2b}$$

$$\rho\left[u\frac{\partial w}{\partial x}+v\frac{\partial w}{\partial y}+w\frac{\partial w}{\partial z}\right] = -\frac{\partial p}{\partial z}+\left[\left[\frac{\partial}{\partial x}\left(\eta\frac{\partial w}{\partial x}\right)+\frac{\partial}{\partial y}\left(\eta\frac{\partial w}{\partial y}\right)+\frac{\partial}{\partial z}\left(\eta\frac{\partial w}{\partial z}\right)\right]\right](z-direction) \tag{2c}$$

Energy equation:

$$\rho C_p\left[u\frac{\partial T}{\partial x}+v\frac{\partial T}{\partial y}+w\frac{\partial T}{\partial z}\right] = k\left[\frac{\partial^2 T}{\partial x^2}+\frac{\partial^2 T}{\partial y^2}+\frac{\partial^2 T}{\partial z^2}\right] \tag{3}$$

The Quemada viscosity model can be defined as follows [29–31]:

$$\eta = K\dot{\gamma}^n(Power-lawmodel) \tag{4}$$

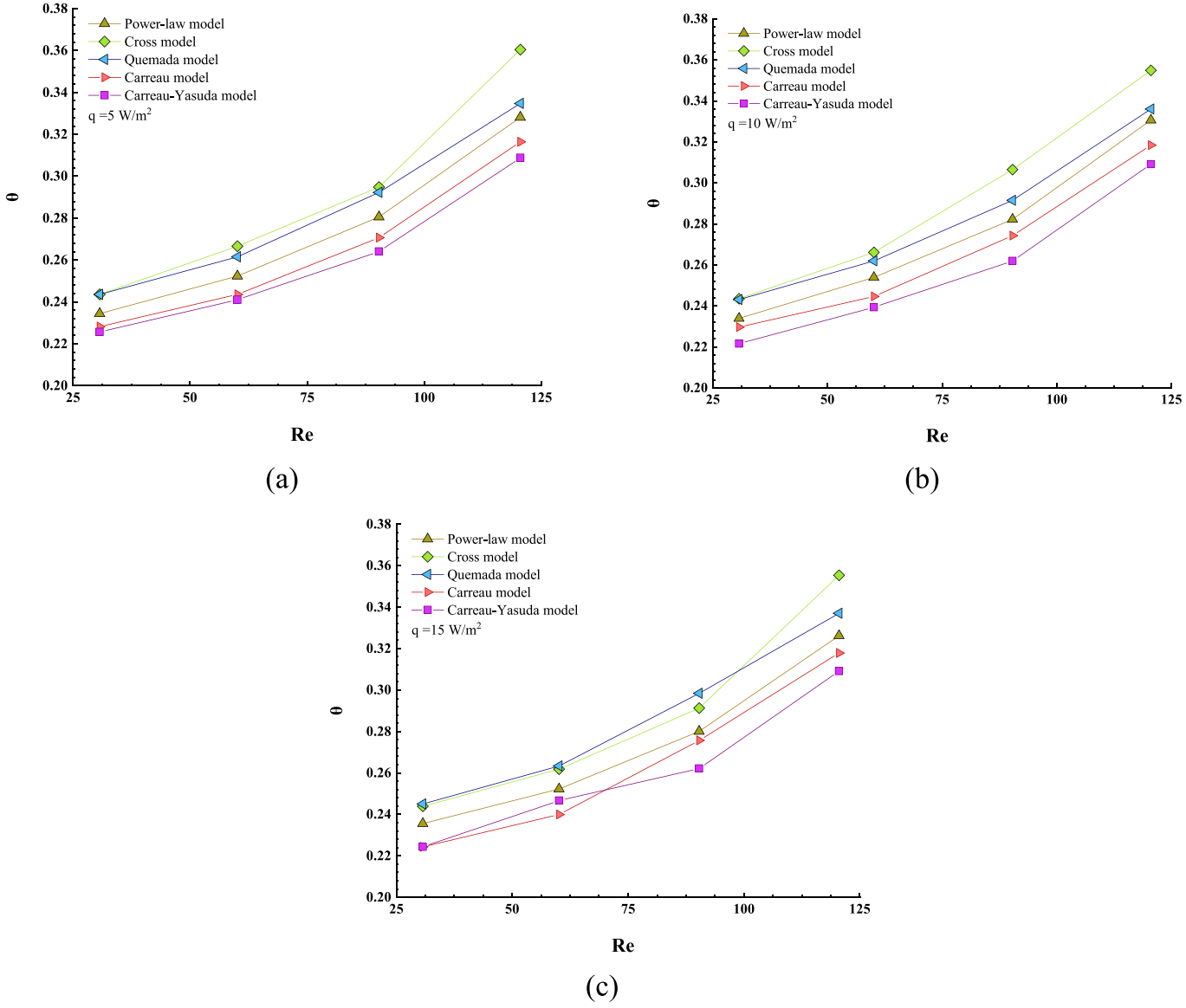

Fig. 4. The θ at various Re in a CBV for all five viscosity.

$$\eta = \eta_\infty + \frac{\eta_0 - \eta_\infty}{1 + \lambda\dot{\gamma}^n}(Crossmodel) \tag{5}$$

$$\eta = \eta_\infty \left[1 - \frac{1}{2}\frac{k_0 + k_\infty\sqrt{\dot{\gamma}/\gamma_c}}{1 + \sqrt{\dot{\gamma}/\gamma_c}}H_t\right]^{-2}(Quemadamodel) \tag{6}$$

$$\eta = \eta_\infty + [\eta_0 - \eta_\infty] - \left[1 + A|\dot{\gamma}|^2\right]^b(Carreaumodel) \tag{7}$$

$$\eta = \eta_\infty + [\eta_0 - \eta_\infty] - \left[1 + [\lambda\dot{\gamma}]^b\right]^{\frac{a-1}{b}}(Carreau - Yasudamodel) \tag{8}$$

where constant parameters are defined as $K = 0.035$, $n = 0.6$, $\eta_\infty = 0.0033$, $\eta_0 = 0.056$, $A = 10.976$, $b = 1.23$, $\lambda = 8.2$ and $a = 0.64$.

The dimensionless parameters are illustrated as follows:

$$\mathrm{X} = \frac{x}{D} - \mathrm{Y} = \frac{y}{D} - \mathrm{Z} = \frac{z}{D} - \theta = \frac{T_b - T_{in}}{T_w - T_{in}} - \Delta\mathrm{p}^+ = \frac{\Delta p}{\Delta p_s} - \mathrm{DAWSS} = \frac{\tau}{\tau_s} \tag{9}$$

The surface integration of each segment calculates the Nu following the heat transfer coefficient (HTC). Moreover, the average Nu is calculated by volume integration of the entire calculation zone.

The local heat transfer coefficient (LHTC) is shown as follows [29]:

$$h(x) = \frac{q''(x)}{(T_w(x) - T_b)} \tag{10}$$

$$T_w(x) = \frac{1}{A}\int TdA \tag{11}$$

$$T_b(x) = \frac{\int T\rho\left|\vec{V}d\boldsymbol{A}\right|}{\int \rho\left|\vec{V}d\boldsymbol{A}\right|} \tag{12}$$

Besides, the average Nu is signified as follows:

$$Nu(x) = \frac{h(x)D_h}{k} \tag{13}$$

$$Nu = \frac{1}{L}\int_0^L Nu(x)dx \tag{14}$$

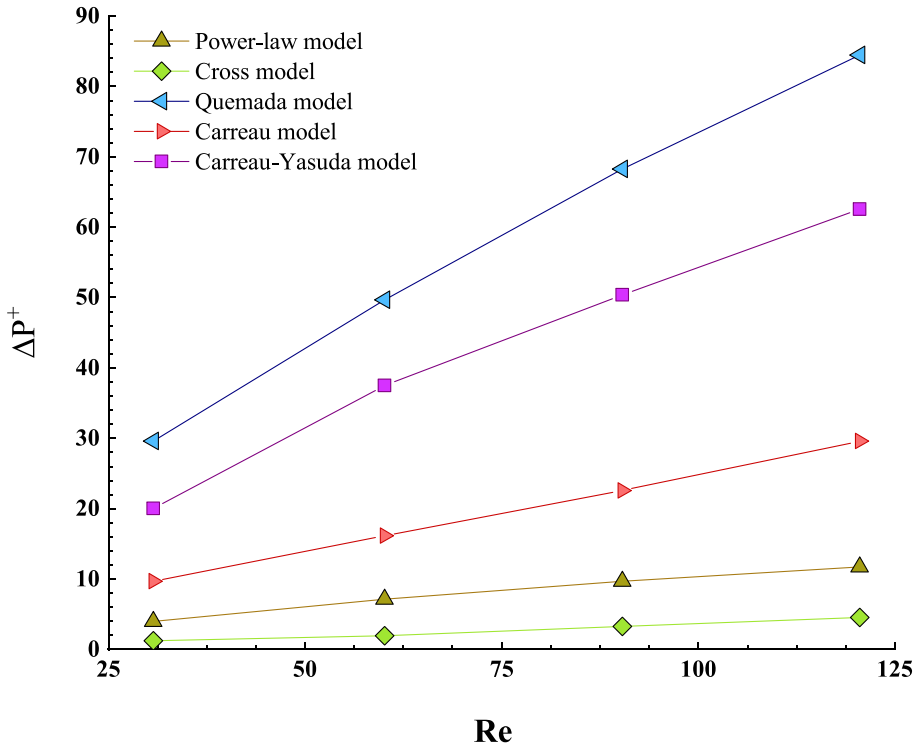

Fig. 5. Change in Δp^{+} at various Re in the CBVs for all five viscosity models.

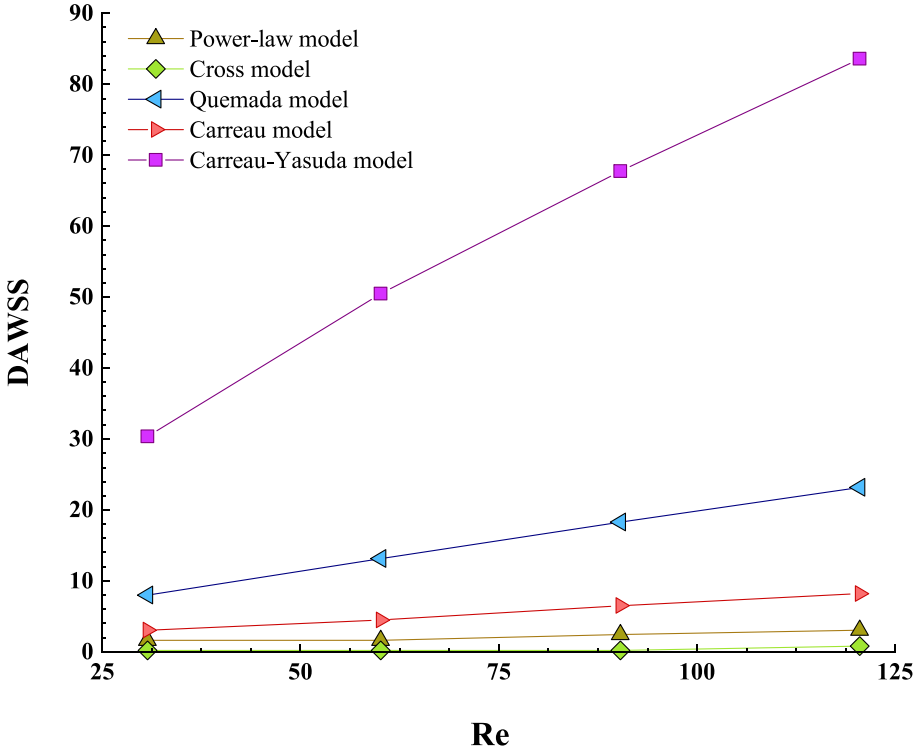

Fig. 6. Changes of DAWSS versus Re in the CBVs for all five viscosity models.

$$Nu = \frac{hD_h}{k} \tag{15}$$

Δp can be measured as follows:

$$\Delta P = \frac{2fL\rho u_{in}^2}{D_h} \tag{16}$$

Finally, the grid independency of the simulated structure is examined. Checking grid independency is one of the most significant parts of any simulation. Generally, it can be expressed that if the simulation study of grid independency is not done in the simulation, the simulation answers are not trustworthy and cannot be mentioned. The grid independence of the 3D model of the simulated CBVs is represented in Fig.2a. The relationship between Re and vessel diameter is about naturally smaller vessels and how smaller diameter affects hemodynamics. Considering that the blood flow is assumed to be laminar. In laminar flow, the pressure changes have a direct relationship with the flow rate and it enhances the growth of the flow speed, but it reaches a constant value in the turbulence region. As a result, it is better to check the Δp in the laminar areas (Fig. 2b).

3. Results and discussion

The impression of the Nu on different Re in the CBVs for three types of heat fluxes produced by the body, consisting of sleeping, standing, and running, are represented in Fig. 3 (from Ref. [27]). This figure also reported the effect of five nNVMs on the Nu. The Nu increases by increasing the entrance velocity because of an extended thermal border layer by increasing the heat produced by the body in various positions. Furthermore, the expansion of the thermal boundary layer is reduced by increasing velocity.

Fig. 4 indicates the θ at different Re amounts in the CBVs for five nNVMs. As mentioned above, the θ enhances with increasing Re in the CBVs (Fig. 4). This can be attributed to two reasons: 1) a faster expanding thermal border layer in the CBVs that reduced the temperature difference between blood flow and the blood vessel wall. This is because some viscosity models represent a higher viscosity than other models, and 2) increasing velocity by enhancing the Re at the entrance. For example, the growth in Re from 60 to 90 in the Carreau-Yasuda viscosity model in the running position of the body leads to a growth in the θ of about 1.1446 times.

Fig. 5 depicts the diagram of Δp^+ in terms of Re in the CBVs for all five nNVMs. As shown, the Δp^+ enhances by increasing the Re. This can be attributed to two main reasons: 1) In some models, with increasing the Re and blood viscosity, the amount of velocity and viscosity of cerebral blood flow increases more than in other models, respectively. And 2) the increasing blood flow viscosity by increasing Δp^+. For example, by enhancing the Re from 90 to 120 in the Cross viscosity model, the Δp^+ changes about 1.391 times.

Fig. 6 shows the DAWSS at different Re in the CBVs, along with the effects of the five nNVMs. The results express that the DAWSS enhances by increasing the Re in all viscosity models. This increase in DAWSS leads to an increasing velocity gradient near the cerebral vessel wall. The increased velocity gradient can increase blood flow viscosity with an increase in some viscosity models than other models and increase Re by changing cerebral blood flow velocity at the entrance.

Figs. 7a and 7b show pressure contours at various Re and velocity contours, respectively. These figures indicate an increase in CBV pressure and velocity with increasing the Re. A rise is observed in Δp at branching parts of the 3D cerebrovascular model. Fig. 7c depicts the velocity streamline contours at various Re and velocity behavior in the geometry. Figs. 7d, 7e, and 7f show the velocity component in each direction.

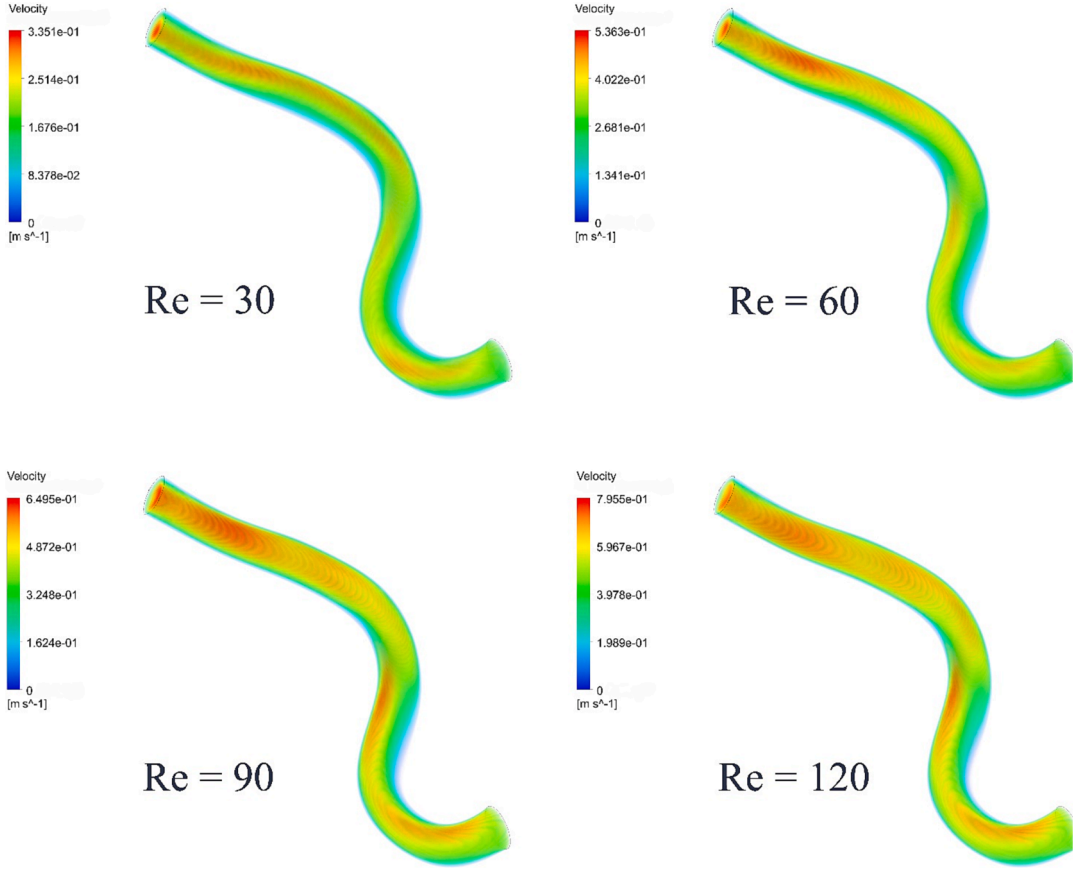

Fig. 7a. The 3D velocity contour at different Re.

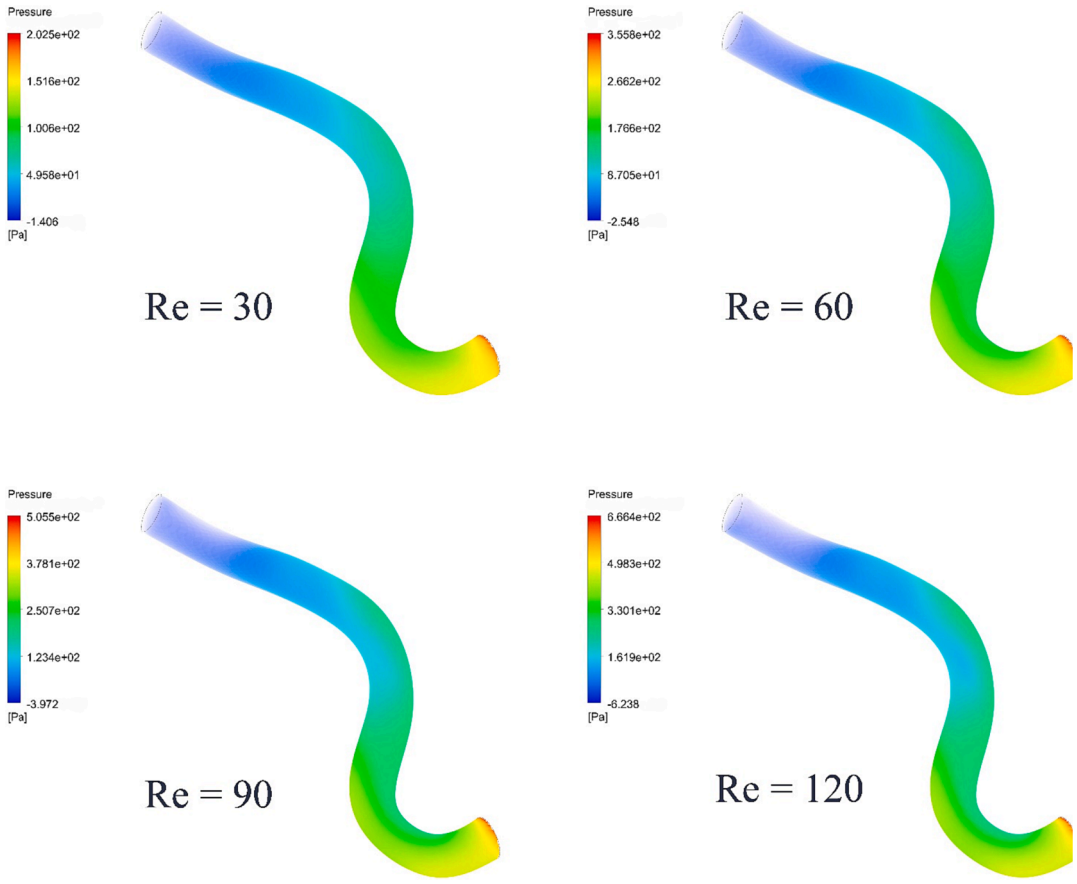

Fig. 7b. The 3D pressure contour at different Re.

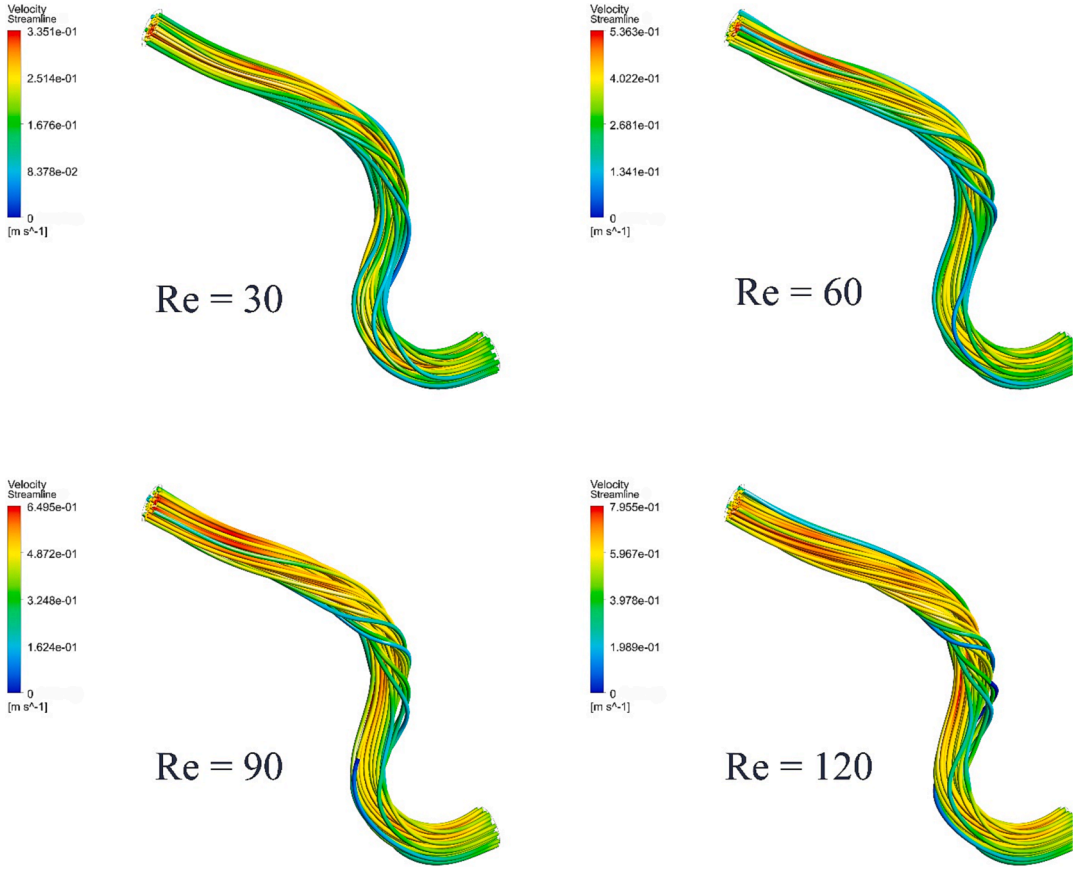

Fig. 7c. The 3D velocity streamlines at different Re.

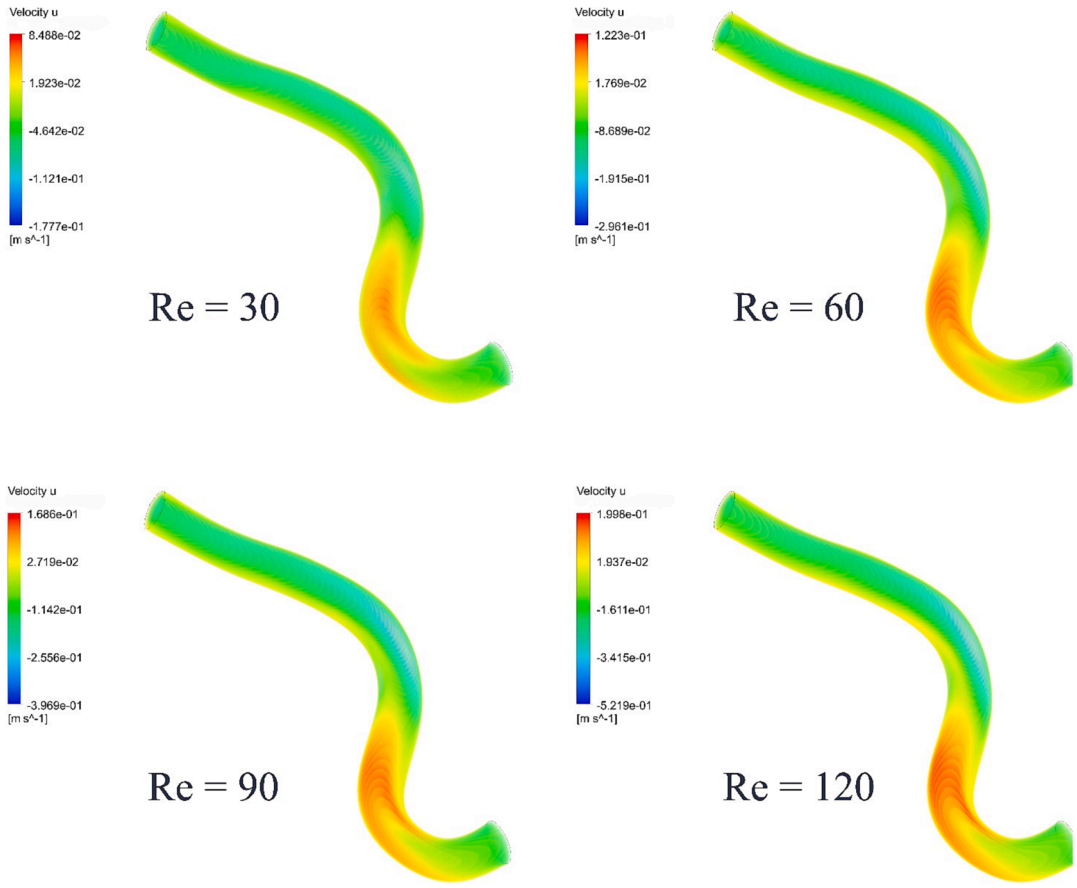

Fig. 7d. The 3D velocity u at different Re.

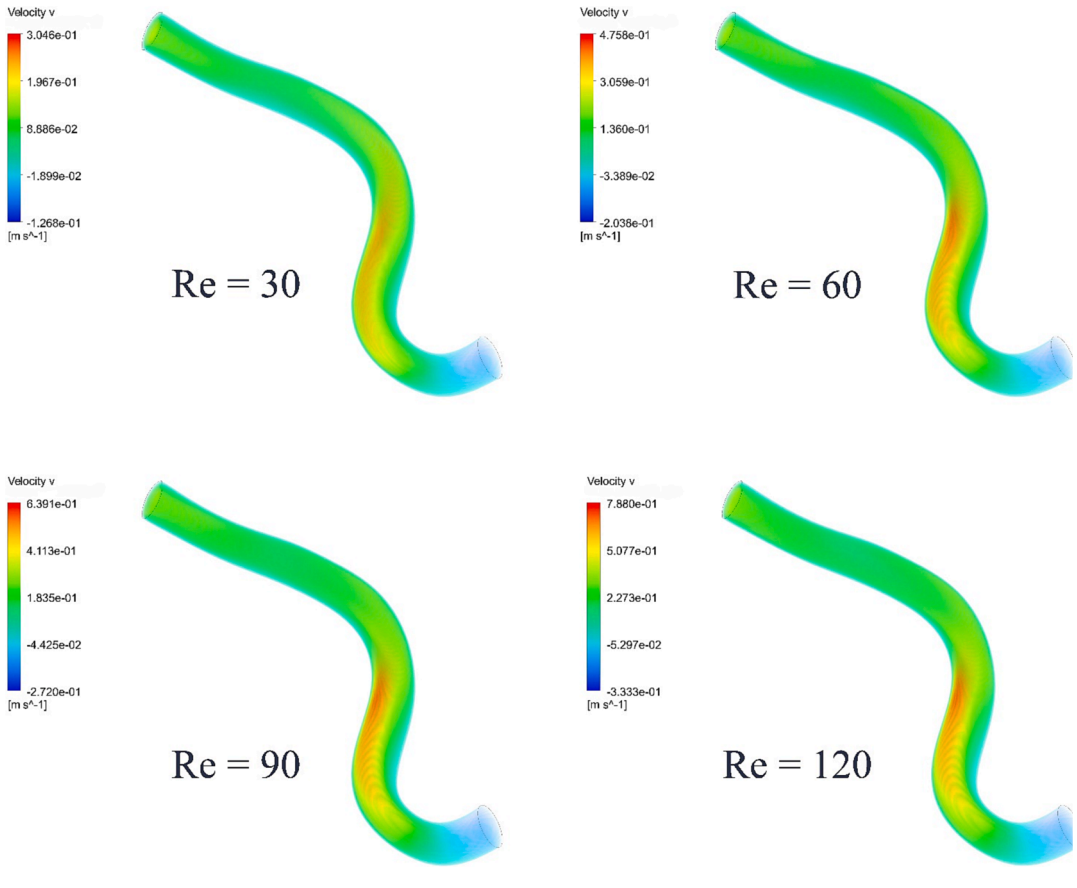

Fig. 7e. The 3D velocity v at different Re.

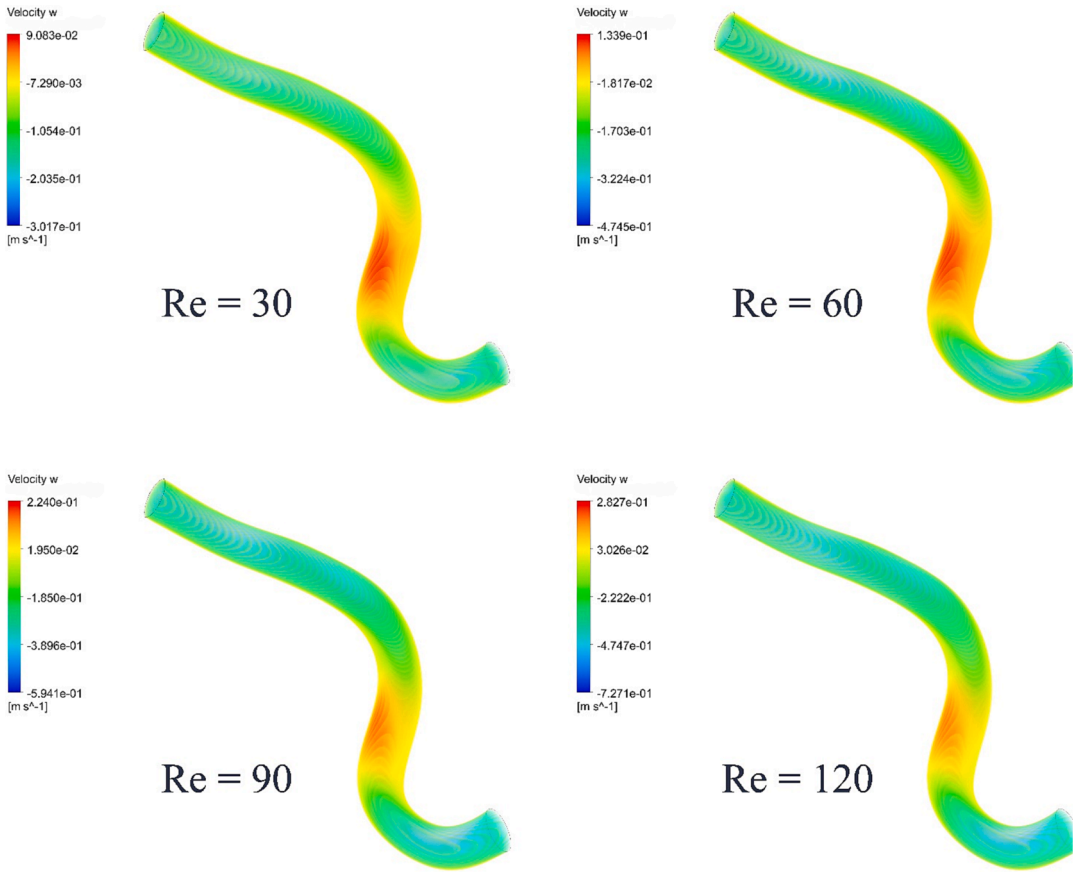

Fig. 7f. The 3D velocity w at different Re.

4. Conclusion

Computational hemodynamics (CHD) is among the most powerful tools to understand blood flow behavior with various nNVMs. It helps the surgeon understand the patient's situation too. The first benefit of this numerical analysis is highlighting the impressions of distinct nNVMs on several parameters in the CBVs and creating geometry with excellent accuracy. The following conclusions can be made:

- The DAWSS enhances by increasing the Re in all viscosity models. This increase in DAWSS leads to an enhancing velocity gradient close to the cerebral vessel wall.
- The increasing Nu is proportionate to the expanding thermal boundary due to increased velocity and viscosity in some viscosity models compared to other models.
- Increasing viscosity by changing the models causes viscous forces to have a greater effect on the CBVs.

Ethics statements

- We certify that all methods were carried out in accordance with proper guidelines and regulations.
- We certify that all experimental protocols were approved by an Islamic Azad University committee.
- We certified that informed consent was achieved from all subjects.

Declaration of Competing Interest

The authors declare that they have no known competing financial interests or personal relationships that could have appeared to influence the work reported in this paper.

References

[1] Standards A, Committee A. Standards for blood banks and transfusion services. Committee on Standards. American Association of Blood Banks; 1974.
[2] Folin O, Wu H. A system of blood analysis. J Biol Chem 1919;38(1):81–110.
[3] Yagi K. [39] Assay for blood plasma or serum. Methods Enzymol 1984;105:328–31.
[4] Edvinsson L, MacKenzie ET, McCulloch J. Cerebral blood flow and metabolism. New York: Raven Press; 1993.
[5] Jain V, Langham MC, Wehrli FW. MRI estimation of global brain oxygen consumption rate. J Cereb Blood Flow Metab 2010;30(9):1598–607.
[6] Scharrer E. The blood vessels of the nervous tissue. Q Rev Biol 1944;19(4):308–18.
[7] Abdel-Halim MS, Lunden I, Cseh G, Änggård E. Prostaglandin profiles in nervous tissue and blood vessels of the brain of various animals. Prostaglandins 1980;19(2):249–58.
[8] Duvernoy HM, Delon S, Vannson J. Cortical blood vessels of the human brain. Brain Res Bull 1981;7(5):519–79.
[9] Nabel EG. Cardiovascular disease. N Engl J Med 2003;349(1):60–72.
[10] Gaziano T, Reddy KS, Paccaud F, Horton S, Chaturvedi V. "Cardiovascular disease," disease control priorities in developing countries. 2nd ed. 2006.
[11] Liu G-T, Wang X-J, Ai B-Q, Liu L-G. Numerical study of pulsating flow through a tapered artery with stenosis. Chin J Phys 2004;42(4):401–9.
[12] Sankar D, Lee U. Mathematical modeling of pulsatile flow of non-Newtonian fluid in stenosed arteries. Commun Nonlinear Sci Numer Simul 2009;14(7):2971–81.
[13] Shaw S, Murthy P, Pradhan S. The effect of body acceleration on two dimensional flow of Casson fluid through an artery with asymmetric stenosis. Open Conserv Biol J 2010;2(1).
[14] Ismail Z, Abdullah I, Mustapha N, Amin N. A power-law model of blood flow through a tapered overlapping stenosed artery. Appl Math Comput 2008;195(2):669–80.
[15] Tarumi T, Zhang R. Cerebral blood flow in normal aging adults: cardiovascular determinants, clinical implications, and aerobic fitness. J Neurochem 2018;144(5):595–608.
[16] Pase MP, Grima NA, Stough CK, Scholey A, Pipingas A. Cardiovascular disease risk and cerebral blood flow velocity. Stroke 2012;43(10):2803–5.
[17] Jennings JR, Heim AF, Kuan D-C-H, Gianaros PJ, Muldoon MF, Manuck SB. Use of total cerebral blood flow as an imaging biomarker of known cardiovascular risks. Stroke 2013;44(9):2480–5.
[18] Moitoi AJ, Shaw S. Magnetic drug targeting during Caputo-Fabrizio fractionalized blood flow through a permeable vessel. Microvasc Res 2022;139:104262.

[19] Shaw S, Sutradhar A, Murthy P. Permeability and stress-jump effects on magnetic drug targeting in a permeable microvessel using Darcy model. J Magn Magn Mater 2017;429:227–35.
[20] Shukla R, Kashaw SK, Jain AP, Lodhi S. Fabrication of Apigenin loaded gellan gum–chitosan hydrogels (GGCH-HGs) for effective diabetic wound healing. Int J Biol Macromol 2016;91:1110–9.
[21] Sharma B, Kumawat C, Makinde O. Hemodynamical analysis of MHD two phase blood flow through a curved permeable artery having variable viscosity with heat and mass transfer. Biomech Model Mechanobiol 2022;21(3):797–825.
[22] Das S, Barman B, Jana R, Makinde O. Hall and ion slip currents' impact on electromagnetic blood flow conveying hybrid nanoparticles through an endoscope with peristaltic waves. BioNanoScience 2021;11(3):770–92.
[23] Prakash O, Makinde O, Singh S, Jain N, Kumar D. Effects of stenoses on non-Newtonian flow of blood in blood vessels. Int J Biomath 2015;8(01):1550010.
[24] Updegrove A, Wilson NM, Merkow J, Lan H, Marsden AL, Shadden SC. SimVascular: an open source pipeline for cardiovascular simulation. Ann Biomed Eng 2017;45(3):525–41.
[25] Deng T, Liu X, Zhang Y, Naghdi S. Erythrocytes number in healthy individuals and anaemia laminar blood flow in the Ulnar vein in both men and women: The analysis of multi-phase heat transfer for medical application. Alex Eng J 2022;61 (12):10099–107.
[26] Ahmadikia H, Moradi A, Fazlali R, Parsa AB. Analytical solution of non-Fourier and Fourier bioheat transfer analysis during laser irradiation of skin tissue. J Mech Sci Technol 2012;26(6):1937–47.
[27] Yan S-R, Sedeh S, Toghraie D, Afrand M, Foong LK. Analysis and manegement of laminar blood flow inside a cerebral blood vessel using a finite volume software program for biomedical engineering. Comput Methods Programs Biomed 2020; 190:105384.
[28] Kavusi H, Toghraie D. A comprehensive study of the performance of a heat pipe by using of various nanofluids. Adv Powder Technol 2017;28(11):3074–84.
[29] Barnoon P, Toghraie D. Numerical investigation of laminar flow and heat transfer of non-Newtonian nanofluid within a porous medium. Powder Technol 2018;325: 78–91.
[30] Mimouni Z. The rheological behavior of human blood—comparison of two models. Open Journal of Biophysics 2016;6(02):29.
[31] Jahangiri M, Saghafian M, Sadeghi MR. Effect of six non-Newtonian viscosity models on hemodynamic parameters of pulsatile blood flow in stenosed artery. J Comput Appl Res Mech Eng (JCARME) 2018;7(2):199–207.